Thermodynamic limit in the elastic triangle: Padé approximants

A. H. Opie
School of Applied Mathematics, University of New South Wales, Sydney, Australia

J. Grindlay
Physics Department, University of Waterloo, Waterloo, Ontario, Canada N2L 1A5

(Received 16 August 2001; published 11 April 2002)

The equilibrium properties of a triangular pile of N rows of particles, interconnected by linear springs and subjected to gravity are explored. A preliminary algebraic investigation of the small N value case suggests that the particle displacement field can be represented by low order Padé approximants. [1,1] Padé approximant representations are introduced for the horizontal and vertical displacement field components. Each representation contains three polynomials in the particle position coordinates. In the vertical displacement case the polynomials are successfully fitted to numerical solutions of the equilibrium equations. The resulting expression exhibits a thermodynamic limit with $1/N$ corrections. This procedure fails in the horizontal case. It is suspected that a higher order Padé approximant is required.

DOI: 10.1103/PhysRevE.65.041303 PACS number(s): 45.05.+x, 01.55.+b

I. INTRODUCTION

In two earlier papers [1,2] we discussed the equilibrium properties of a triangular pile of particles, interconnected by linear springs and subjected to the force of gravity. In Ref. [1] the equilibrium state was determined from a numerical analysis of the particle equilibrium conditions. The results showed (a) an unexpected richness in behavior in a simple model and (b) evidence of a thermodynamic limit [3,4] in triangles with ≈100 layers. Previous work [5–8] on the thermodynamic limit has been restricted to homogeneous systems in uniform equilibrium states. With the pile model we have a quite different situation, namely, a homogeneous system in nonuniform equilibrium. In the second paper, Ref. [2], we attempted to obtain an algebraic solution to the equilibrium problem of the triangle of particles. We used perturbation theory based on the supposition that some springs are weaker than others. The zero order solutions did exhibit thermodynamic limit behavior; we found that corrections to the thermodynamic limit dropped inversely as the number of rows of particles in the triangular array. In contrast, the first order solutions turned out to be unsatisfactory, in as much as the expansion parameter proved to be a function of the size of the triangle—an inappropriate result for a thermodynamic limit discussion.

In the present paper we describe another attempt to obtain an algebraic solution to the equilibrium conditions. We return to the homogeneous model of Ref. [1] and explore, using MAPLE™, the algebraic nature of the equilibrium solution. We are restricted by computing capacity considerations to sizes of triangles well below the thermodynamic limit seen in Ref. [1]. However, the results we obtain suggest that Padé approximants [9,10] could provide suitable representations to describe the equilibrium solutions for triangles beyond the algebraic scope of MAPLE™. We explore this avenue using a mixture of [1,1] Padé approximants and numerical solutions to the equilibrium conditions. This tactic proves to be satisfactory for the field describing the vertical shifts of the particles but is unsatisfactory for the horizontal shifts. To our knowledge, this is first reported use of Padé approximants in a thermodynamic limit discussion.

The triangle model and the equilibrium conditions are described in the following section. The results of the MAPLE™ analysis are given in Sec. II A. The Padé approximant is introduced in Sec. II B and applied to the problem of the horizontal and vertical shifts in Secs. II C, II D, and II E. Section III contains a brief summary of our results.

Model

Consider a regular, triangular array of particles with N rows. We label the rows $n=1,2,\ldots,N$ and the particles within a row from the left $s=1,2,\ldots,n$, Fig. 1. Each particle has a common mass m and is connected to its six neighbors by linear springs. The springs have equilibrium lengths a, a' and spring constants λ, λ'; the inner angle is θ. We introduce a set of Cartesian axes with origin in the middle of the base, x_1 axis through the base particles and x_2 axis through the apex. The parameters a, a', θ can be used to introduce scaled position coordinates,

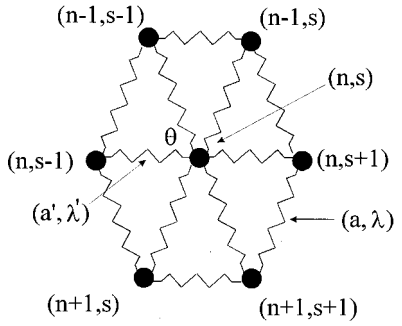

FIG. 1. Triangular array of particles and springs in equilibrium in the absence of gravity. The rows are labeled, $n=1,2,\ldots,N$ and the particles within rows are labeled $s=1,2,\ldots,n$. The bottom row, $n=N$, is in contact with a solid smooth line. The springs connecting particles between rows are characterized by unstretched length a, spring constant λ, and the in row springs by (a',λ').

$$x_1=(2s-n-1)/N, \quad x_2=(N-n)/N, \tag{1}$$

with scale factors, $Na\cos\theta$, $Na\sin\theta$, respectively, see Ref. [2]. Thus the particle at the lower right-hand corner has coordinates $(1-1/N,0)$ and that at the apex coordinates (0,1).

This two-dimensional plane array of particles is in equilibrium under the actions of the unstretched springs. Now let us suppose that (a) gravity is switched on and acts in the direction of the negative x_2 axis and (b) the bottom layer of particles is supported to prevent any vertical motion of the row of $n=N$ particles. The particles have new equilibrium positions. Let the shift in equilibrium of the (n,s)th particle be denoted by the dimensionless pair of components $[u_1(s,n),u_2(s,n)]$, with scale factors, $(mg/\lambda)/(\sin\theta\cos\theta)$ and $(mg/\lambda)/\sin^2\theta$, respectively, see Ref. [2]: g is the acceleration due to gravity. These displacements are determined by the set of equilibrium conditions for the particles in the triangular array. For an interior particle the equilibrium conditions take the form, see Ref. [2] in the horizontal direction

$$\begin{aligned}0=\gamma&[u_1(n,s+1)-2u_1(n,s)+u_1(n,s-1)]+[u_1(n-1,s)\\&+u_1(n-1,s-1)+u_1(n+1,s)+u_1(n+1,s+1)\\&-4u_1(n,s)]+[u_2(n-1,s)-u_2(n-1,s-1)\\&+u_2(n+1,s)-u_2(n+1,s+1)],\end{aligned} \tag{2}$$

and in the vertical direction

$$\begin{aligned}1=&[u_1(n-1,s)-u_1(n-1,s-1)+u_1(n+1,s)\\&-u_1(n+1,s+1)]+[u_2(n-1,s)+u_2(n-1,s-1)\\&+u_2(n+1,s)+u_2(n+1,s+1)-4u_2(n,s)],\end{aligned} \tag{3}$$

where

$$\gamma=\lambda'\sec^2\theta/\lambda. \tag{4}$$

The spring constants λ, λ' are positive quantities and hence $\gamma\geqslant 0$. The equilibrium conditions for particles on the edges of the triangle have different forms from Eqs. (2), (3). They can be found in Ref. [1].

The solutions to the equilibrium conditions for the $N(N+1)/2$ particles are functions of position coordinates x_1, x_2, pile size N, and the ratio γ, Eq. (4). The effect of gravity occurs through the displacement scale factors listed in the previous paragraph.

II. PADÉ APPROXIMANTS [9,10]

A. Algebraic solutions

The program MAPLE™ can be used to obtain explicit algebraic expressions for the solutions to the triangle equilibrium conditions for $N\leqslant 20$. Utilizing this program we find the following results.

The equilibrium solutions are of the form

$$u_1(x_1,x_2,\gamma)=\frac{N^2}{\gamma}\frac{\phi_1^N(x_1,x_2,\gamma)}{\phi_0^N(\gamma)},$$

$$u_2(x_1,x_2,\gamma)=\frac{N^2}{\gamma}\frac{\phi_2^N(x_1,x_2,\gamma)}{\phi_0^N(\gamma)}, \tag{5}$$

where the ϕ's are polynomials in the parameter γ of the form

$$\phi_0^N=\sum_{l=0}^{r} c_l^{(0)}\gamma^l, \tag{6}$$

$$\phi_1^N=\sum_{l=0}^{r} c_l^{(1)}(x_1,x_2)\gamma^l, \tag{7}$$

and

$$\phi_2^N=\sum_{l=0}^{r+1} c_l^{(2)}(x_1,x_2)\gamma^l. \tag{8}$$

The upper limits for the sums are

$$r=N(N-2)/4, \quad N \text{ even} \quad \text{and} \quad r=(N-1)^2/4, \quad N \text{ odd}. \tag{9}$$

We may think of ϕ_1^N, ϕ_2^N as fields within the triangle.

In the case of ϕ_0^N and fixed N, the coefficients $c_l^{(0)}$ increase in magnitude with increasing index l until about $l\sim r/2$ and then decrease. The maximum value of $c_l^{(0)}$ increases dramatically with increasing size of N. For example, in the case $N=8$, ϕ_0^8 is a polynomial of degree 12; the maximum coefficient has a value $\approx 10^4$ and occurs for the γ^8 term. In the case $N=20$, the polynomial is of degree 90 and the maximum coefficient has a value $\approx 10^{10}$ for the γ^{17} term. In the case of the other two ϕ's, ϕ_1^N, ϕ_2^N, the sets coefficients $c_l^{(1)}$, c_l^2 vary across the triangle, (7), (8) but exhibit the same pattern, i.e., maximum values occurring at about $l\sim r/2$ and dramatic increases with increasing N.

We know from the numerical solutions described in Ref. [1] that the fields ϕ_1^N/ϕ_0^N and ϕ_2^N/ϕ_0^N are independent of N for large enough N. This result appears, at first sight, to be at odds with the polynomial properties noted above, (significant changes with increasing N). To explore this point further, consider the special case of the displacement of the corner

TABLE I. Real roots of the two polynomials ϕ_0^8 and ϕ_0^8 [Eq. (5)].

ϕ_0	ϕ_1
−0.1685	−0.1659
−0.2644	−0.2997
−0.4411	
−0.6048	
−0.7318	−0.7870
−1.1435	
−1.3959	−1.3958
−2.6707	−2.6881
−3.0734	
−6.7707	−8.1921
−13.3870	−13.7176
−25.6843	−25.5090

TABLE II. Exact and approximate results for the horizontal displacement of the (N,N) particle for four different N's and two different spring constant ratios. All the results were obtained from MAPLE™.

N	Solution	$\gamma=0.4$	$\gamma=4.0$
8	Exact	0.232 757 704 2	0.027 146 109 70
	[5,5]	0.232 757 704 7	0.027 146 098
	[1,1]	0.2331	0.027 07
12	Exact	0.241 222 774	0.029 390 667 44
	[5,5]	0.242 122 279 8	0.029 390 58
	[1,1]	0.242 69	0.029 23
16	Exact	0.247 139 395 2	0.030 744 348 42
	[5,5]	0.247 139 399 1	0.030 744 21
	[1,1]	0.247 83	0.030 51
20	Exact	0.250 318 383 5	0.031 650 637 41
	[5,5]	0.250 318 389 0	0.031 650 24
	[1,1]	0.2511	0.031 35

particle, (N,N) in the triangle with $N=8$. For this particle $u_2=0$ and ϕ_0^8, ϕ_1^8 are polynomials of degree 12 in γ. The real roots of ϕ_0^8, ϕ_1^8 are given in Table I. We note that (a) all the roots of ϕ_0 are negative and (b) for most of the roots of ϕ_0 there is a similarly sized root in ϕ_1. We discuss the consequences of (a) in the Appendix. Given property (b) and positive values of γ (the appropriate physical range for a ratio of two positive elastic constants), we can expect an approximate cancellation of these pairs in the ratio ϕ_0^8/ϕ_1^8. This ''approximate cancellation'' reduces the ratio of two high order polynomials to a ratio of two lower order polynomials. Similar results were obtained for different sizes of triangles. In our view the cancellation process described above is a likely explanation of the thermodynamic limit behavior seen in general in the ratios of polynomials in Eq. (5) [1]. We note that the three polynomials, ϕ_0^N, ϕ_1^N, and ϕ_2^N are simply related to an equilibrium matrix array and its cofactors, see the Appendix, and thus the thermodynamic limit behavior is a direct consequence of properties of this matrix. The cancellation process also suggests that one might seek displacement representations in terms of ratios of low order polynomials in γ. This is a well-recognized technique; the ratios are referred to as Padé approximants [9,10].

To explore the feasibility of a Padé approximant representation, consider again the corner particle (N,N) with displacement u_1. We used MAPLE™ to obtain an explicit power series expression in $(\gamma-1)$ for the quantity $\gamma u_1/N^2 = \phi_1^N/\phi_0^N$, Eq. (5). We then applied the MAPLE™ Padé package to this series to calculate the [1,1] and [5,5] Padé approximants. We show the results for two different γ values and four different triangle sizes N in Table II. From this data we see that the [1,1] Padé approximant represents the displacement with better than 1% accuracy.

As we have noted above, the MAPLE™ algebraic program will not give solutions to the equilibrium conditions for $N>20$, i.e., well before the thermodynamic limit behavior seen in Ref. [1]. To explore the properties of displacements in larger piles our strategy will be to (a) represent the horizontal and vertical displacements with [1,1] Padé approximants and (b) determine the position and N dependence of the corresponding six functions from various numerical solutions to the equilibrium conditions. With this approach we hope to explore, in particular the manner in which the system reaches the thermodynamic limit.

B. Padé approximants

We assume that the displacement solutions to the pile equilibrium conditions can be written in the [1, 1] Padé form

$$u_z(x_1,x_2,N,\gamma) = \frac{N^2}{\gamma}\left[H_z(x_1,x_2,N)\,\frac{1+(\gamma-1)K_z(x_1,x_2,N)}{1+(\gamma-1)L_z(x_1,x_2,N)}\right], \quad z=1,2. \tag{10}$$

Thus, in this approximation, u_1, u_2 are described by six functions, H_1, H_2, K_1, K_2, L_1, and L_2. In the special case $\gamma=1$, Eq. (10) reduces to

$$u_z(x_1,x_2,N,1)=N^2H_z(x_1,x_2,N), \quad z=1,2. \tag{11}$$

Thus Eq. (10) can be rewritten in the form

$$u_z(x_1,x_2,N,\gamma)=\frac{u_z(x_1,x_2,N,1)}{\gamma}\,\frac{1+(\gamma-1)K_z(x_1,x_2,N)}{1+(\gamma-1)L_z(x_1,x_2,N)} \quad z=1,2. \tag{12}$$

C. H_1 and H_2

The equilibrium conditions for an $N=116$ triangle with $\gamma=1$ were solved numerically with a Gauss-Seidel scheme [11]. Equilibrium data, correct to seven places, were obtained for the case of a 116 layer triangle (about 5000 iterations are needed to achieve this accuracy). The resulting 3 335 values of u_1/N^2 for $x_1\geqslant 0$ were used to generate the contour plot shown by the solid lines in Fig. 2, These contours describe the function $H_2(x_1,x_2,N=116)$, Eq. (11). The analogous results for the vertical displacement function $H_1(x_1,x_2,N=116)$ are shown in Fig. 3.

We investigated the N dependence of H_1, H_2 (for fixed x_1, x_2) in the following fashion. Consider the particle with labels $n=58$, $s=44$ in the $N=116$ triangle. This particle has coordinates (1/8,1/2), Eq. (1). As we reduce the size of N, we find no particle with *precisely* these coordinates until we reach the value 108. In this triangle the particle with labels $n=54$, $s=41$ has these coordinates. In general, if the layer number has the form

$$N=8p+4, \quad p=1,2,3,\ldots, \tag{13}$$

then the particle with labels

$$n=4p+2, \quad s=3p+2, \quad p=1,2,3,\ldots \tag{14}$$

has coordinates position coordinates (1/8, 1/2), see the line fourth in Table III. The equilibrium conditions for the 11

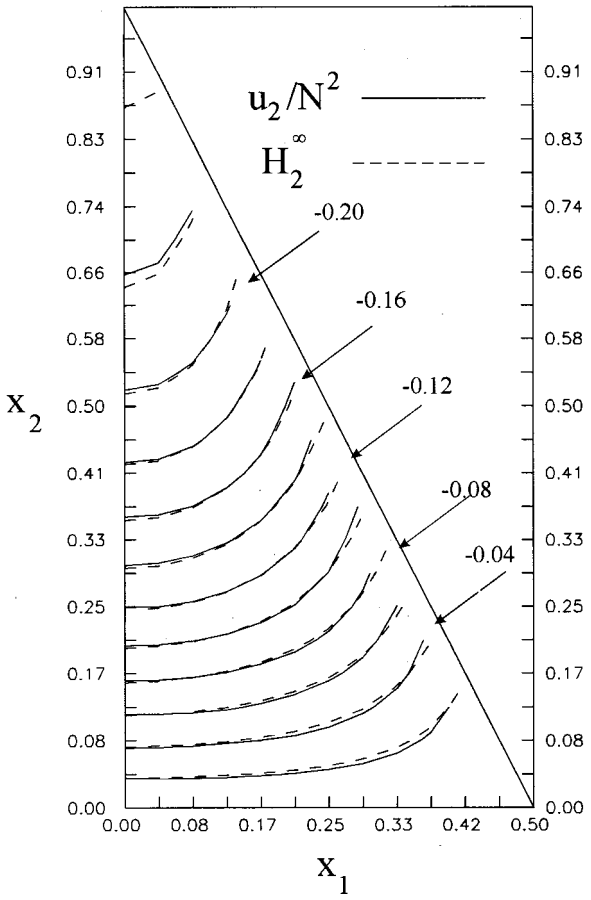

FIG. 2. Solid lines depict a contour map of the vertical displacement field scaled by $1/N^2$. The field values are obtained from numerical solutions to the equilibrium conditions, (2), (3) plus (20), (21), (22) in Ref. [1] for the case $N=116$, $\gamma=1$. The dashed lines depict a contour plot of the function H_2^{∞} described by the six term polynomial representation, Eq. (21). The coefficients in this representation are determined by the leading term in the limiting form (15) for each of the vertical displacements in the last six lines of Table III.

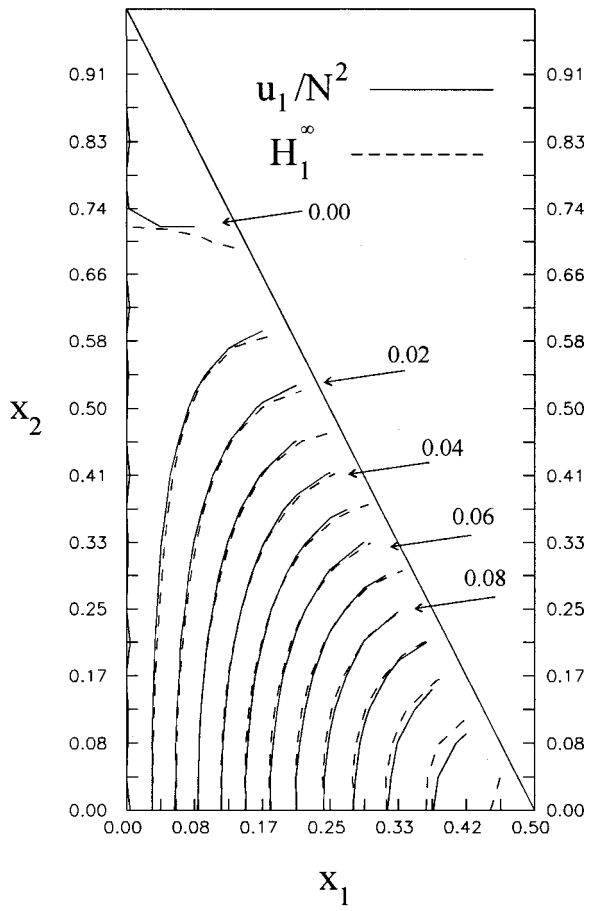

FIG. 3. Solid lines depict a contour map of the horizontal displacement field scaled by $1/N^2$. The field values are obtained from numerical solutions to the equilibrium conditions, (2), (3) plus (20), (21), (22) in Ref. [1] for the case $N=116$, $\gamma=1$. The dashed lines depict a contour plot of the function H_1^{∞} described by the six term polynomial representation, Eq. (20). The coefficients in this representation are determined by the leading term in the limiting form (17) for each of the horizontal displacements in the first six lines of Table III.

triangles with $N=108$ to $N=20$ in steps of eight were solved numerically with the Gauss-Seidel scheme. The 12 values of $H_2(1/8,1/2,N)$ are shown in Fig. 4. The straight line through the larger values is described by the function

$$H_2=H_2^{\infty}+H_2'/N, \tag{15}$$

with parameters

$$H_2^{\infty}=-0.1837, \quad H_2'=0.1109. \tag{16}$$

The analogous results for the horizontal displacements are also shown in Fig. 4. The straight line is described by the function

$$H_1=H_1^{\infty}+H_1'/N, \tag{17}$$

with parameters

$$H_1^{\infty}=0.016\,592, \quad H_2'=-0.014\,018. \tag{18}$$

We note that, from these data

$$H_z\cong H_z^{\infty}, \quad z=1,2, \tag{19}$$

to better than 1% for $N>100$ and the corrections to the thermodynamic limit drop off inversely with N.

There are other points in the triangle with precisely the same coordinates as we vary the layer number N by certain amounts. We list other seven in Table III. The same process was carried out for each of these points and obtained similar results; at each position in the triangle both H_2 and H_1 have the form of Eqs. (15) and (17), respectively, and the relation (19) holds (to better than 1%) at the maximum N value used, see Table III. If, as seems likely, Eq. (19) holds at each point in a large ($N>100$) triangle the solid line contour maps in Figs. 2 and 3 describe the position dependence of H_2^{∞} and H_1^{∞}, respectively. Because the contours in Figs. 2 and 3 are smooth, slowly varying functions of position we attempted to represent H_2^{∞} and H_1^{∞} by six term polynomials in x_1, x_2.

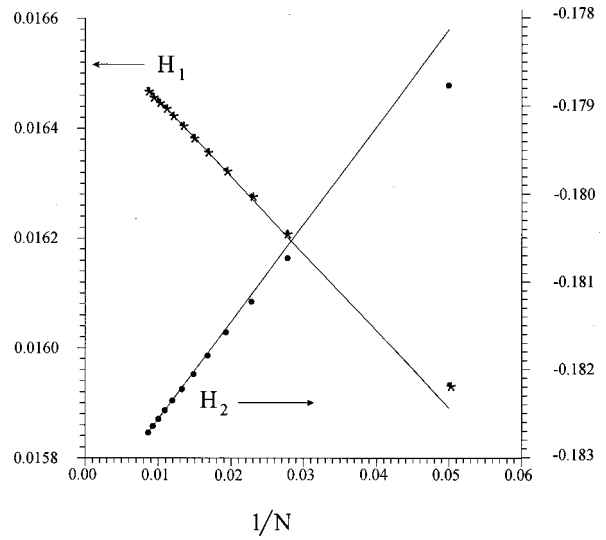

FIG. 4. The asterisks indicate the points $(H_1\ 1/N)$, left-hand scale. $H_1=u_1/N^2$, where u_1 is the numerical solution to the equilibrium conditions for the position (1/8,1/2) in the triangles with $N=28,36,\ldots,116$. The straight line, Eq. (17), passes through the $N=116,108$ points with slope and intercept (18). The filled circles are obtained from the analogous vertical case with right-hand axis, straight line (15) and slope and intercept (16).

Consider the properly symmetrized forms

$$H_1^{\infty}=a_{10}x_1+a_{11}x_1x_2+a_{12}x_1x_2^2+a_{30}x_1^3+a_{13}x_1x_2^3+a_{31}x_1^3x_2, \tag{20}$$

$$H_2^{\infty}=a_{01}x_2+a_{02}x_2^2+a_{03}x_2^3+a_{21}x_1^2x_2+a_{04}x_2^4+a_{22}x_1^2x_2^2. \tag{21}$$

The six coefficients in Eq. (20) were determined by equating this function with each of the set of six H_1^{∞} values obtained from the horizontal displacement data for the points in the first six lines of Table III, The six coefficients in Eq. (21) were obtained in a similar fashion from the vertical displacement data for the last six lines in Table III. The values of the coefficients are shown in Table IV. With these values we generated the dashed contours in Figs. 2 and 3. We conclude from these two figures that, aside from regions near the perimeter of the triangle, the six term polynomials, Eqs. (20) and (21), give good representations for H_1^{∞} and H_2^{∞}. We also fitted the two coefficients H_1', H_2', Eqs. (15) and (17), to six term polynomials cf. Eqs. (20) and (21) using the data from the first six and last six points, respectively, in Table III. The polynomial coefficients are given in Table IV. The resulting contour maps of H_2', H_1' are shown in Figs. 5 and 6. It is interesting to note that $H_1'\approx -1.2H_1^{\infty}$ and $H_2'\approx -0.6H_2^{\infty}$ at each point in the triangle, compare Figs. 3 and 5 and Figs. 4 and 6.

TABLE III. Points in the triangle used to generate the polynomial representations for the functions appearing in the [1,1] Padé approximant forms. The entries in the second column generate, $p=1,2,3,\ldots$, the triangles in which there is a particle sitting exactly on the point in the position in the first column. The third and fourth columns contain the corresponding n and s values. The last column contains the largest N value used in the thermodynamic limit fitting, (15), (17), (24), (25).

Point	N	n	s	N max
(1/4,0)	$4p+2$	$4p+2$	$3p+2$	114
(1/3,0)	$6p+3$	$6p+3$	$5p+3$	117
(1/12,2/3)	$12p+6$	$4p+2$	$3p+2$	114
(1/8,1/2)	$8p+4$	$4p+2$	$3p+2$	116
(1/6,1/3)	$6p+3$	$4p+2$	$3p+2$	117
(3/10,1/5)	$10p+5$	$8p+4$	$7p+4$	125
(0,1/2)	$4p+2$	$2p+1$	$p+1$	114
(0,1/4)	$8p+4$	$6p+3$	$3p+2$	116

D. K_2 and L_2

To determine the functions in the numerator and denominator of the Padé approximant form in Eq. (10) at a given point x_1,x_2 in a given triangle N, we calculate the three displacements $u_z(x_1,x_2,N,1)$, $u_z(x_1,x_2,N,\gamma)$, and $u_z(x_1,x_2,N,\gamma')$, with $\gamma\neq\gamma'\neq 1$ and use these values to solve Eq. (12) for the pair K_z,L_z.

For example, we numerically calculated the vertical displacements at the point (1/8,1/2) in the $N=116$ triangle for the three values $\gamma=1.1,1.0,0.9$. Using Eq. (12) we find

$$K_2=0.632\,84\pm 0.000\,03,\quad L_2=0.0179\pm 0.000\,03. \tag{22}$$

The error estimates in Eq. (22) are a consequence of the uncertainty in the eighth place in the original equilibrium data. Equation (12) is based on the assumption of a [1,1] Padé approximant for the displacement, Eq. (10). As a check on the assumption in this case we adopted the values in Eq. (22) and used Eq. (10) to calculate the displacements at the point (1/8,1/2) for $N=116$ and a variety of γ values. We then compared the results with the corresponding displacements obtained from a numerical solution of the equilibrium equations. As a measure of the error we introduce the quantity

$$\Delta=\frac{u_2^P(x_1,x_2,N,\gamma)}{u_2(x_1,x_2,N,\gamma)}-1, \tag{23}$$

where u_2^P is the Padé approximant, Eq. (10), [with $H_2\cong H_2^{\infty}$ given in Eq. (16) and K_2,L_2 given by Eq. (22)] and u_2 the vertical displacement obtained from a numerical solution to the equilibrium conditions. The results of the check are shown in Table V. We see that, at this point in the triangle, the [1,1] Padé approximant is good to 1% or better for γ in the range [0.4,4].

This calculation was repeated for each of the remaining 3421 particles with $x_1\geqslant 0$, in the 116 layer triangle. K_2,L_2 were calculated from the $\gamma=1.1,1.0,0.9$ displacements, see Eq. (12). The results are shown as contour plots in Figs. 7 and 8. As a check on the validity of the Padé approximation, we calculated the error measure, Eq. (23), for the 3422 particles in the triangle with $\gamma=4$. All but 15 particles had error measures less than 0.05. The 15 particles lie in the lower right corner of the triangle and have errors in the range

TABLE IV. Coefficients of the polynomial representations for H_1^∞, H_2', H_1^∞, H_2', K_2^∞, K_2', L_2^∞, and L_2' defined in Eqs. (17), (15), (24), and (25).

	x_1	x_1x_2	$x_1x_2^2$	x_1^3	$x_1x_2^3$	$x_1^3x_2$
H_1^∞	0.3720	0.1404	−1.8083	−0.5080	1.2224	−0.6046
H_1'	−0.6439	0.5717	1.8171	0.5642	−1.8191	1.3044
	x_2	x_2^2	x_2^3	$x_1^2x_2$	x_2^4	$x_1^2x_2^2$
H_2^∞	−0.5409	0.082 86	0.6243	2.4306	−0.4254	−1.1262
H_2'	0.3893	0.1067	−1.2864	−2.8064	0.9990	2.5131
	1	x_2	x_2^2	x_1^2	$x_1^2x_2$	x_2^3
K_2^∞	0.7184	−0.3096	0.2221	0.7180	0.6084	−0.0301
K_2'	−0.8706	5.775	−13.210	1.3852	−3.8568	9.563
L_2^∞	0.007 56	0.1947	−0.4648	−0.1556	0.2498	0.2440
L_2'	−.6797	6.171	−13.674	−0.1698	−1.7302	9.686

(0.05,0.63). For $\gamma=0.4$ a similar calculation yields 28 particles in the lower right corner with errors in the range (0.05,0.25); the remaining error measures are less than 0.05. We conclude that, for 99.2% of the particles in the triangle, the [1,1] Padé approximant, Eq. (10), represents the vertical displacements to better than 5% in the range $0.4 \leqslant \gamma \leqslant 4.0$.

To begin the discussion of the large N behavior of K_2, L_2, we consider again the particle at the point (1/8,1/2). The values of K_2, L_2 for $N=116$ are given in Eq. (22). We repeated this calculation for the same point for each of the six triangles with $N=108$ to $N=68$ in steps of eight, see Eqs. (13), (14), and the associated discussion. The K_2, L_2 values

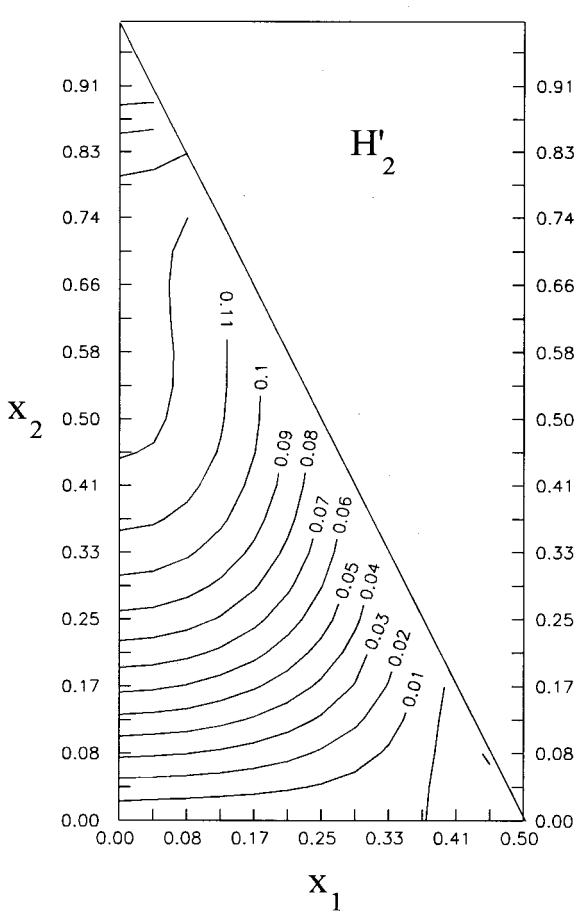

FIG. 5. A contour plot of the function H_2' described by the six term polynomial representation, Eq. (21). The coefficients in this representation are determined by the H_2' term in the limiting form (15) for each of the vertical displacements in the last six lines of Table III.

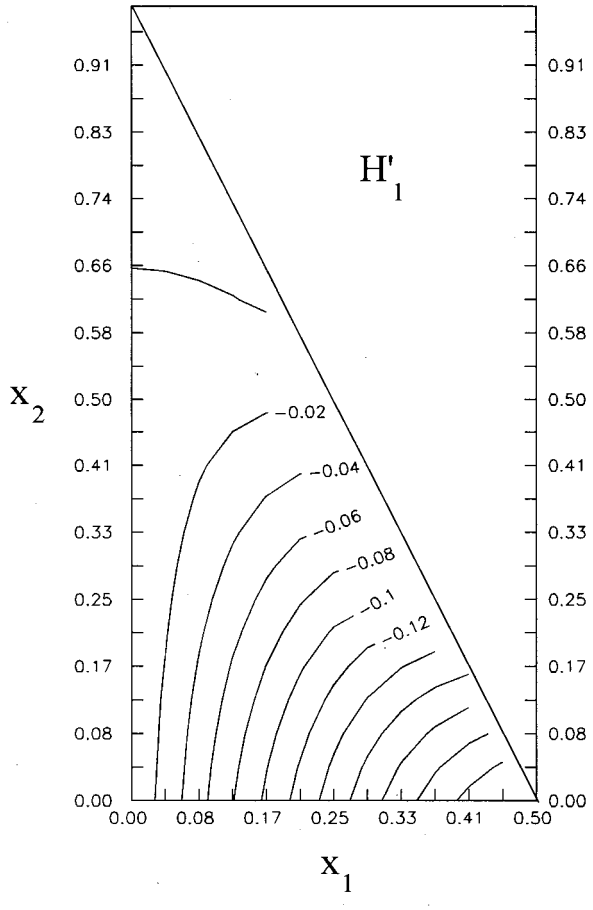

FIG. 6. A contour plot of the function H_1' described by the six term polynomial representation, Eq. (20). The coefficients in this representation are determined by the H_1' term in the limiting form (17) for each of the horizontal displacements in the first six lines of Table III.

TABLE V. Error, Eq. (23), in the [1,1] Padé approximant, Eq. (10), for the vertical displacement at the point (1/8,1/2) in the triangle $N=116$ for different spring constant ratios. The K_2, L_2 values, Eq. (22), are calculated from the displacements when $\gamma=1.1,1.0,0.9$.

γ	4.0	2.0	1.3	1.2	0.8	0.7	0.4
Δ	-1.2×10^{-2}	-2.4×10^{-3}	-1.1×10^{-4}	-3.0×10^{-5}	4.9×10^{-5}	2.3×10^{-4}	3.4×10^{-3}

are plotted as functions of $1/N$ in Figs. 9 and 10. From these graphs we conclude that for large triangles at the point (1/8,1/2)

$$K_2=K_2^{\infty}+K_2'/N, \tag{24}$$

$$L_2=L_2^{\infty}+L_2'/N, \tag{25}$$

with

$$K_2^{\infty}=0.6312\pm0.0002, \quad K_2'=0.180.02, \tag{26}$$

$$L_2^{\infty}=0.0185\pm0.0001, \quad L_2'=-0.07\pm0.005. \tag{27}$$

The same process was carried out for the vertical displacements of the remaining five of the last six points listed in Table III. We find that at each point K_2 and L_2 have the forms shown in Eqs. (24) and (25). However, in contrast to the H-function case, see Eq. (19), at $N\approx100$, K_2 differs from K_2^{∞} by about 5% and L_2 from L_2^{∞} by about 20%. The six values of K_2^{∞} were fitted to a six term polynomial representation of the form

$$K_2^{\infty}=b_{00}+b_{01}x_2+b_{02}x_2^2+b_{20}x_1^2+b_{21}x_1^2x_2+b_{03}x_2^3. \tag{28}$$

The calculated coefficients are shown in Table IV. We carried out the same fitting process for K_2',L_2^{∞},L_2'. The corre-

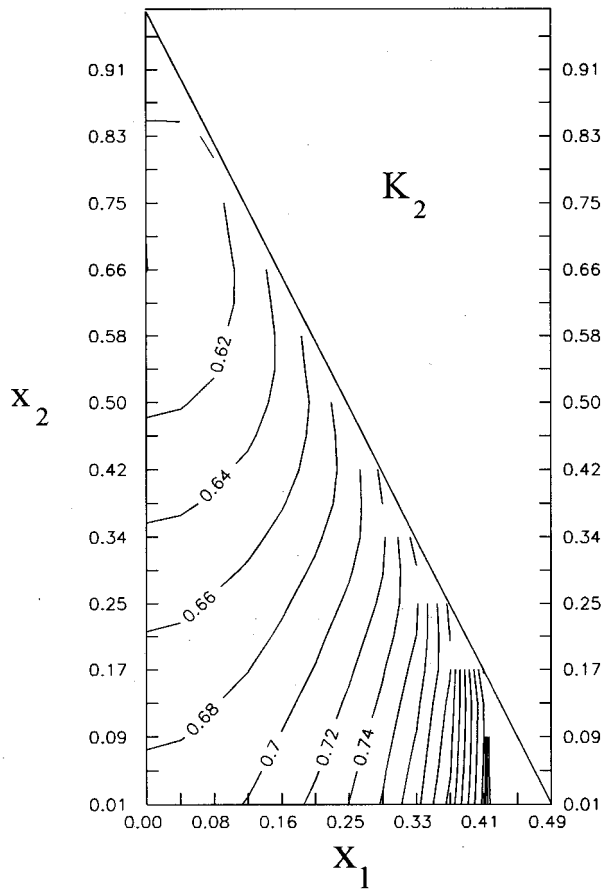

FIG. 7. A contour plot of the quantity K_2 in the Padé [1,1] approximant for the vertical displacement, Eq. (10). The K_2 values used to generate this map were obtained by solving for K_2 and L_2 from Eq. (12) using the vertical displacement for $\gamma=1.1,1.0,0.9$ at each of the 3421 particles in the right side of the $N=116$ triangle.

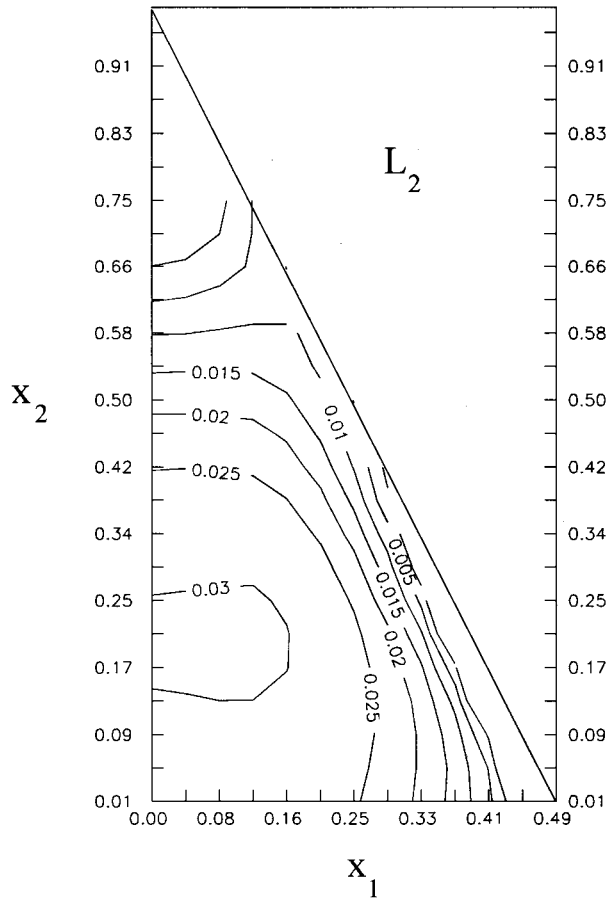

FIG. 8. A contour plot of the quantity L_2 in the Padé [1,1] approximant for the vertical displacement, Eq. (10). The L_2 values used to generate this map were obtained by solving for K_2 and L_2 from Eq. (12) using the vertical displacement for $\gamma=1.1,1.0,0.9$ at each of the 3421 particles in the right side of the $N=116$ triangle.

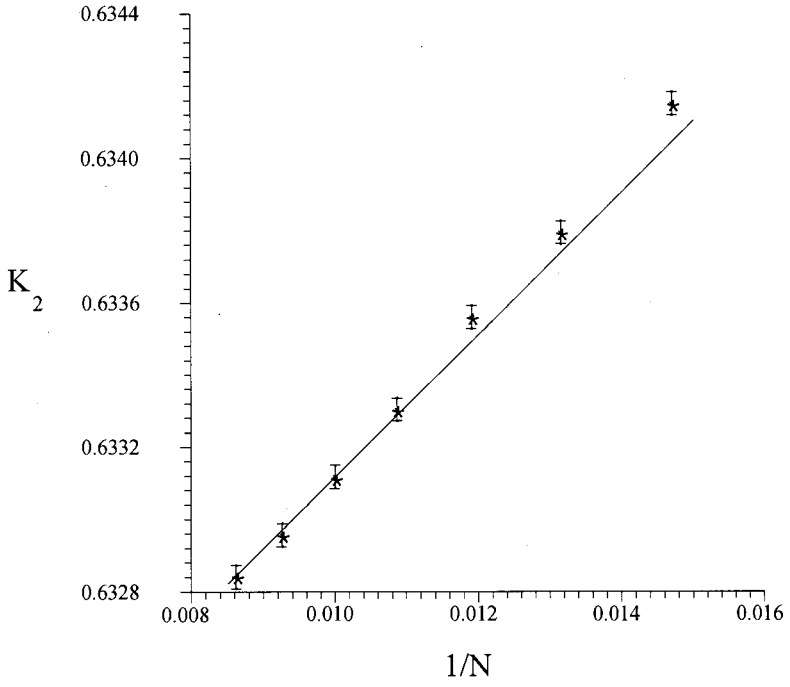

FIG. 9. The asterisks indicate the points $(K_2,1/N)$. K_2 is the Padé [1,1] function, Eq. (10), calculated from the vertical equilibrium displacements for the position (1/8,1/2) in the triangles with $N=68,76,\ldots,116$ and the values $\gamma=1.1,1.0,0.9$. The straight line, Eq. (24), passes through the $N=116,108$ points with slope and intercept, Eq. (26).

sponding coefficients are also given in Table IV. The contour maps generated by the six term polynomial representations for $K_2^{\infty},L_2^{\infty},K_2',L_2'$ are shown in Figs. 11, 12, 13, and 14, respectively.

Figure 7 displays a contour map of K_2 calculated from all the vertical displacements in a triangle with 116 layers; in contrast, Fig. 11 is a contour map of K_2^{∞} generated from a polynomial representation based on the large N behavior of the vertical displacements of six particles. The differences between the two maps are in part due to the fact that $K_2 \approx K_2^{\infty}$ is a poor approximation at $N=116$ and in part due to the inadequacy of a six term polynomial representation, Eq. (28). Similar remarks hold for the pair of maps in Figs. 8 and 12. Here the $L_2 \approx L_2^{\infty}$ approximation is even less satisfactory, see above.

The results described above suggest that the large N behavior of the vertical displacements can be written in the form

$$u_2(x_1,x_2,N,\gamma)=\frac{N^2}{\gamma}[H_2^{\infty}+H_2'/N] \times\left[\frac{1+(\gamma-1)(K_2^{\infty}+K_2'/N)}{1+(\gamma-1)(L_2^{\infty}+L_2'/N)}\right], \quad (29)$$

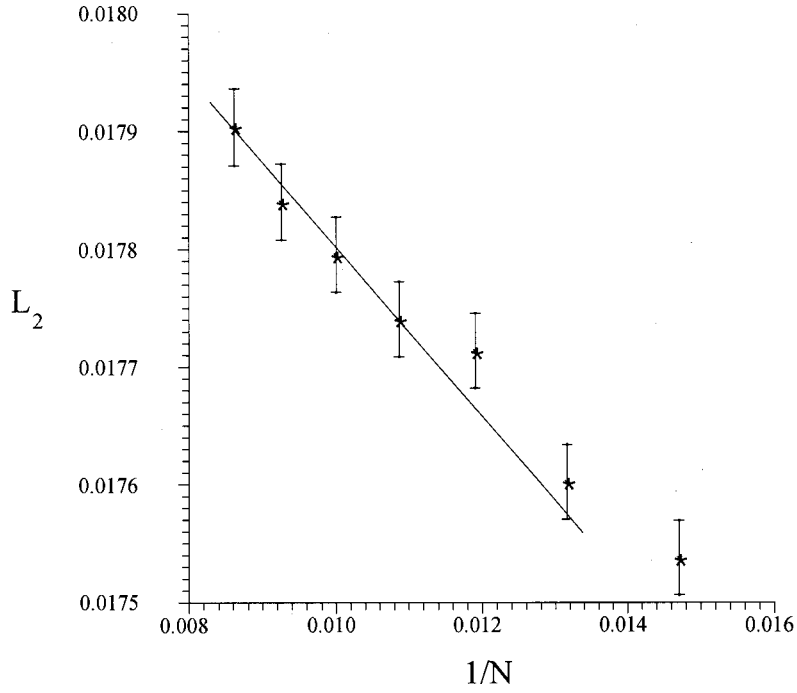

FIG. 10. The asterisks indicate the points $(L_2,1/N)$. L_2 is the Padé [1,1] function, Eq. (10), calculated from the vertical equilibrium displacements for the position (1/8,1/2) in the triangles with $N=68,76,\ldots,116$ and the values $\gamma=1.1,1.0,0.9$. The straight line, Eq. (24), is a least square fit through the points $N=116,108,100,92$ points with slope and intercept, Eq. (26).

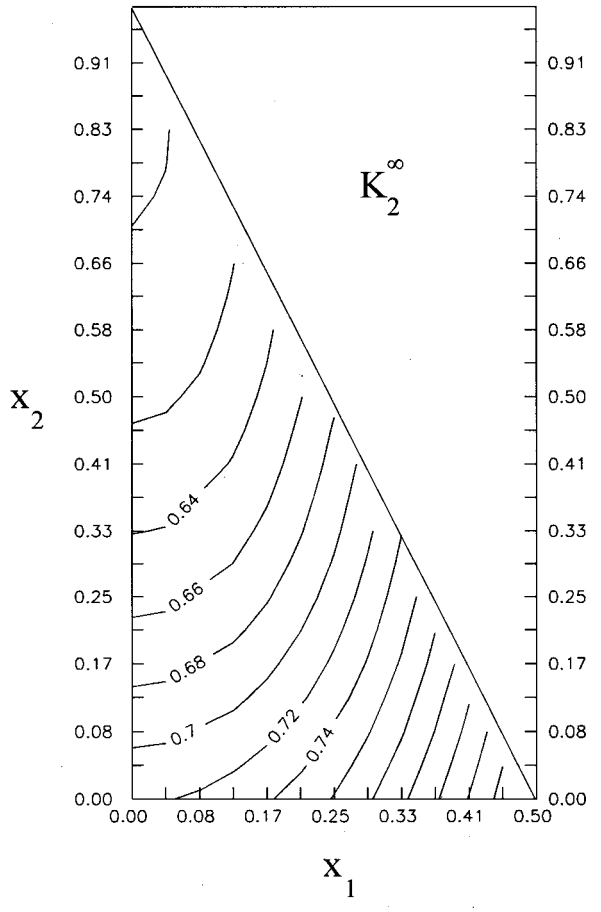

FIG. 11. A contour plot of the function K_2^∞ described by the six term polynomial representation, Eq. (28). The coefficients in this representation are determined by the K_2^∞ term in the limiting form (24) for each of the vertical displacements in the last six lines of Table III.

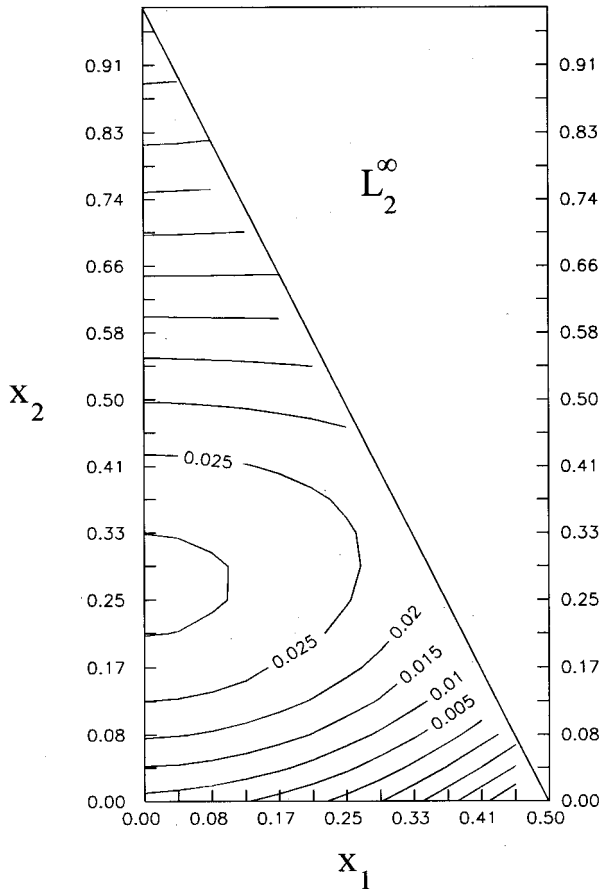

FIG. 12. A contour plot of the function L_2^∞ described by the six term polynomial representation, see Eq. (28). The coefficients in this representation are determined by the L_2^∞ term in the limiting form (25) for each of the vertical displacements in the last six lines of Table III.

where H_2^∞, H_2', K_2^∞, K_2', L_2^∞, and L_2' are functions only of position. Thus in the thermodynamic limit of arbitrarily large N the vertical displacement is

$$u_2^\infty(x_1,x_2,\gamma)=\frac{N^2H_2^\infty(x_1,x_2)}{\gamma}\left[\frac{1+(\gamma-1)K_2^\infty(x_1,x_2)}{1+(\gamma-1)L_2^\infty(x_1,x_2)}\right], \tag{30}$$

and the correction to thermodynamic limit drops off inversely with N. As a check on the adequacy of the six term polynomial representations for $K_2^\infty, K_2', L_2^\infty, L_2'$, Table IV, we used the expression in Eq. (29) plus the polynomial representations to calculate u_2/N^2 for the particles in an $N=116$ triangle and $\gamma=4.0$. The results are shown as dashed lines in the contour map Fig. 15. The solid lines are obtained from a numerical solution of the equilibrium conditions for the same system. The analogous comparison for the case $\gamma=0.4$ is shown in Fig. 16. These two figures indicate that the six term polynomial representations plus the Padé [1,1] form provide an adequate algebraic representation for the vertical displacement field u_2 for γ in the range (0.4,4.0). We expect that additional terms in the polynomial representations would give closer agreement with the numerical solutions to the equilibrium conditions.

E. K_1 and L_1

There are two potential problems with the [1,1] Padé approximant representation in Eq. (10). The first problem is a practical one. If K_z and L_z are close in value, then Eq. (12) gives

$$\gamma u_z(N,\gamma)/u_z(N,1)\cong 1+\frac{(\gamma-1)\delta}{1+(\gamma-1)L_z}, \tag{31}$$

where $K_z=L_z+\delta$ and $|\delta|\ll 1$. When $\delta=0$, K_z and L_z are indeterminate. When δ is very small but not zero, then $\gamma u_z(N,\gamma)/u_z(N,1)$ can differ from unity by an amount comparable to the numerical error in this ratio, i.e., there can be a significant degradation in accuracy when we apply Eq. (12)

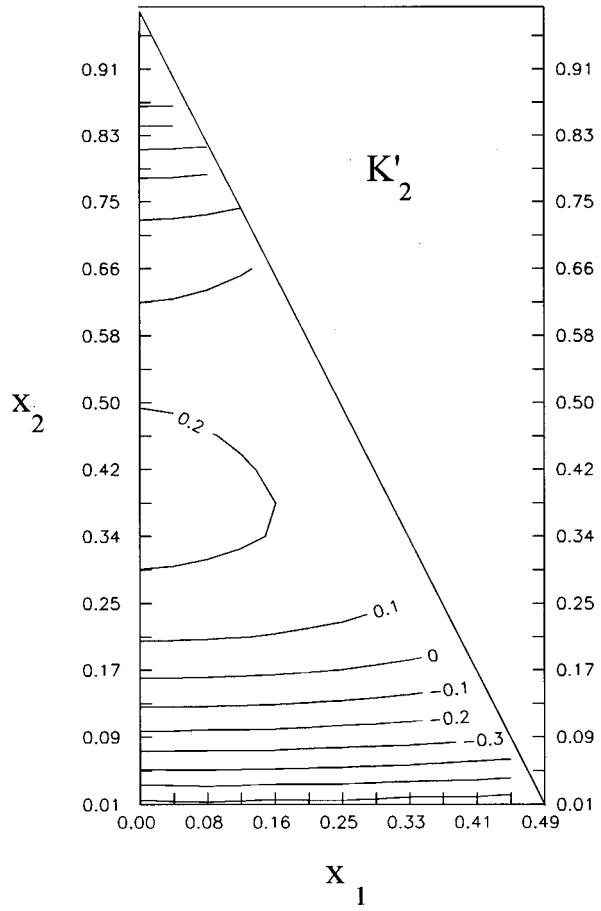

FIG. 13. A contour plot of the function K_z' described by the six term polynomial representation, see Eq. (28). The coefficients in this representation are determined by the K_2' term in the limiting form (24) for each of the vertical displacements in the last six lines of Table III.

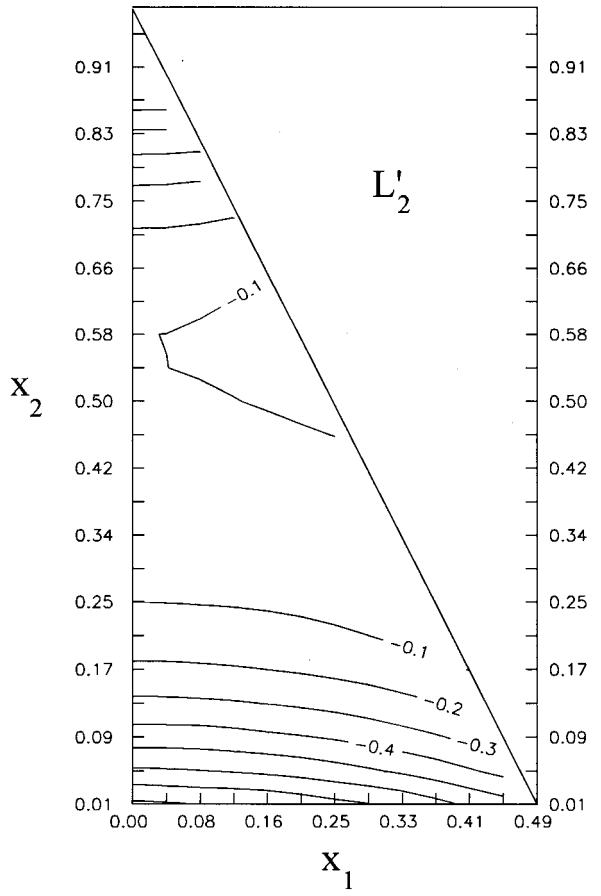

FIG. 14. A contour plot of the function L_2' described by the six term polynomial representation, see Eq. (28). The coefficients in this representation are determined by the L_2' term in the limiting form (25) for each of the vertical displacements in the last six lines of Table III.

to two different γ values to determine K_z and L_z (this is the approach used successfully in the preceding section to obtain K_2, L_2).

The second potential problem is the existence of singularities. If at a given point (x_1, x_2) in a given triangle with N layers,

$$1+(\gamma-1)L_z(x_1,x_2)=0 \tag{32}$$

for some positive value of γ then the [1,1] Padé approximant is infinite and so fails as a representation for the displacement components (which we know to be finite for $\gamma>0$). Equation (32) has the following properties. (i) If $L<0$ then $\gamma>1$, (ii) if $0<L<1$ then $\gamma<0$, (iii) if $1<L$ then $0<\gamma<1$. Since the physics of the system requires $\gamma>0$, there is a potential for a singular [1,1] Padé approximant only when $L<0$ and $1<L$.

In the case of the vertical displacements $0<L_2<1$ and L_2 is distinctly smaller than K_2 everywhere in the triangle and hence neither of these problems occurs in the vertical displacement field.

In contrast, both problems occur in the horizontal displacement case. Following the approach described in Sec. II D, we calculated the horizontal displacements for $\gamma=1.1,1.0,0.9$ and used them to determine the quantities K_1, L_1 for each particle in the right side of the triangle $N=116$. Three significant observations were made.

(a) Along the line $x_2=1/4$, $K_1 \approx L_1$. As a consequence, significant loss of accuracy occurred in the region about this line.

(b) The contour maps of K_1 and L_1 are distinctly more convoluted than those for K_2 and L_2, Figs. 7 and 8. As a result, six term polynomial representations are likely to be quite inadequate.

(c) There are regions in the triangle in which $L_1<0$ and other regions in which $1<L_1$. These give rise to a number of singular Padé approximant representations in the range $0.4 \leqslant \gamma \leqslant 4.0$.

While (a) and (b) are merely computational inconveniences, which could be circumvented, observation (c) destroys the viability of the [1,1] Padé approximant as a representation

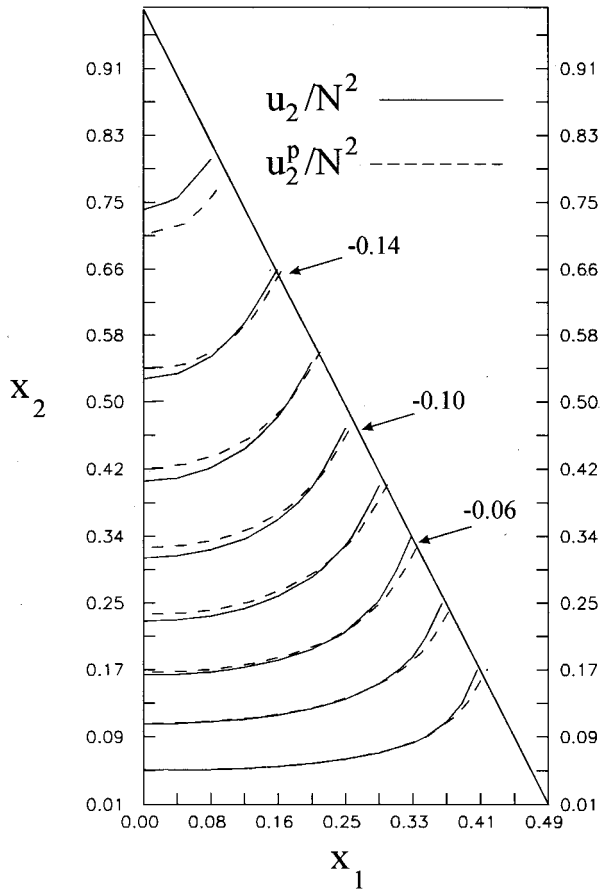

FIG. 15. Contour map; solid lines describe the field u_2/N^2 calculated from the equilibrium conditions for the $N=116$ and spring constant ratio $\gamma=4.0$; dashed lines describe the field u_2^p/N^2 calculated from the [1,1] Padé approximant form, Eq. (10), with the polynomial representations for H_2^∞, H_2', K_2^∞, K_2', L_2^∞, L_2', see Table IV, and $N=116$.

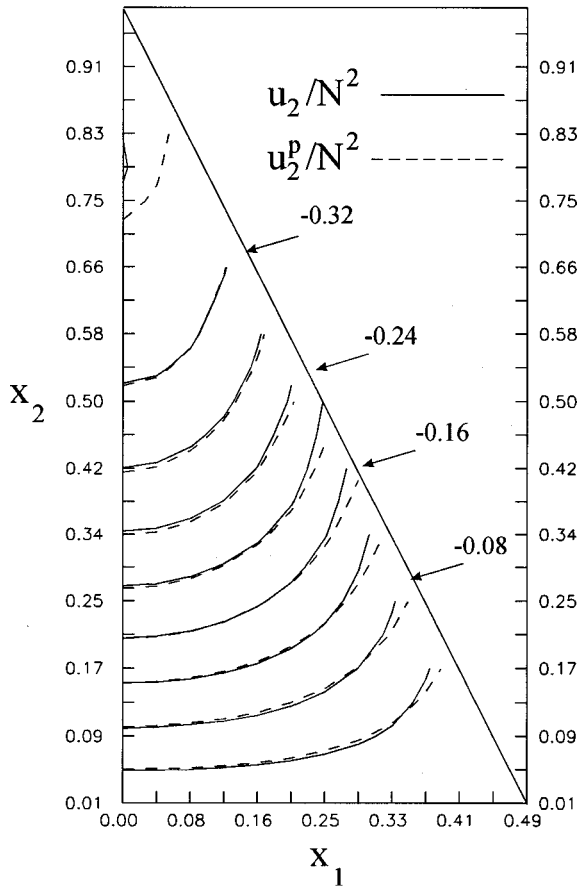

FIG. 16. Contour map; solid lines describe the field u_2/N^2 calculated from the equilibrium conditions for the $N=116$ and spring constant ratio $\gamma=0.4$; dashed lines describe the field u_2^p/N^2 calculated from the [1,1] Padé approximant form, Eq. (10), with the polynomial representations for H_2^∞, H_2', K_2^∞, K_2', L_2^∞, L_2', see Table IV, and $N=116$.

for the horizontal displacement field. If we are to use Padé approximants for u_1, it must be of higher order. In view of the singularity problem in [1,1], the [1,2] approximant is the most likely candidate [12]. We shall not pursue this problem here.

III. SUMMARY

We have explored the feasibility of (a) equating the equilibrium displacement shifts in the N layer triangle of particles with [1,1] Padé approximants and (b) representing the functions in the approximants by six term polynomials in the position coordinates of the particles. The program worked satisfactorily for the vertical shifts. We were able to show that (a) these shifts increase as N^2 and (b) the three fields characteristic of the [1,1] approximant approach limits independent of N for large N. The correction terms drop off as $1/N$. In the case of the horizontal shifts, the [1,1] Padé approximant fails because of the presence of singularities in the ratio of spring constants γ.

ACKNOWLEDGMENT

One of us (J. G.) would like to thank the School of Applied Mathematics at the University of New South Wales for generous support.

APPENDIX

Consider the dynamics of the particles in the triangle introduced in section Model. Let the dimensionless displacement vector, $[u_1(s,n),u_2(s,n)]$, describe the motion of the s,nth particle relative to the equilibrium condition in the absence of gravity. If we introduce the multidimensional vector

$$\vec{\eta}=[u_1(1,1),u_2(1,1),u_1(2,1),u_2(2,1),\ldots,u_1(N,N),u_2(N,N)] \tag{A1}$$

then we can then write the equations of motion for the triangle particles in the form

$$\ddot{\vec{\eta}} = \mathbf{M}(\gamma)\,\vec{\eta} + \vec{g}, \tag{A2}$$

where $\mathbf{M}$ is a square matrix describing the spring interactions between the particles, see Eqs. (2), (3) and the edge conditions in Ref. [1]. It is a function of the spring constant ratio γ; $\vec{g}$ is a vector describing the dimensionless gravitational force acting on the particles. It has the form, $\vec{g} = [0,1,0,1,0,\ldots,0,1]$.

In equilibrium $\vec{\eta} = \vec{\eta}^0$, where

$$\vec{\eta}^0 = -\mathbf{M}^{-1}\vec{g} \tag{A3}$$

or

$$\vec{\eta}^0 = -\frac{\mathbf{m}(\gamma)}{\det[\mathbf{M}(\gamma)]}\vec{g}, \tag{A4}$$

where $\mathbf{m}(\gamma)$ is the matrix array of the cofactors of $\mathbf{M}(\gamma)$. If we compare this expression with the equivalent result in Eq. (5) above, we conclude that

$$\text{(a)} \qquad \gamma\phi_0^N(\gamma) \propto \det\mathbf{M} \tag{A5}$$

and (b) ϕ_1^N, ϕ_2^N are each proportional to an appropriate linear combinations of cofactors of $\mathbf{M}$. Thus the γ dependence of the two ratios $\phi_1^N/\phi_0^N, \phi_2^N/\phi_0^N$ are a direct consequence of the γ dependence of the matrix $\mathbf{M}$. Further, if ϕ_0^N remains positive, i.e., nonzero, for all positive values of the spring constant ratio, γ, then the triangle under gravity has no singular equilibrium displacement solutions.

Let us now consider small oscillations about this equilibrium state. Set

$$\vec{\eta} = \vec{\eta}^0 + \Delta\,\vec{\eta}\exp(i\omega t). \tag{A6}$$

Then the normal mode frequencies are solutions to the eigenvalue problem

$$\det|\mathbf{M} - \omega^2\mathbf{I}| = 0. \tag{A7}$$

In particular, the product of all the eigenvalues is equal to the determinant of the matrix, i.e.,

$$\prod_{i=1}^{s} \omega_i^2 = \det\mathbf{M}, \tag{A8}$$

where $s = N(N+1)/s$ and ω_i is the ith normal mode frequency. Thus if ϕ_0^N remains positive for all positive values of the spring constant ratio, γ, then the state described by the solution $\vec{\eta}^0$ is a stable equilibrium state for all positive values of γ.

[1] A. H. Opie and J. Grindlay, Phys. Rev. E **51**, 724 (1995).
[2] A. H. Opie and J. Grindlay, Physica A **303**, 119 (2002).
[3] A. Munster, *Statistical Thermodynamics* (Springer, New York, 1969), Vol. 1.
[4] I. Catto, C. Le Bris, and P-L. Lions, *The Mathematical Theory of Thermodynamic Limits: Thomas-Fermi Type Models* (Clarendon, Oxford, 1998).
[5] M. E. Fisher, Arch. Ration. Mech. Anal. **17**, 377 (1964).
[6] R. B. Griffiths, J. Math. Phys. **6**, 1447 (1965).
[7] M. E. Fisher and D. Ruelle, J. Math. Phys. **7**, 377 (1966).
[8] E. H. Lieb and J. L. Lebowitz, Adv. Math. **9**, 316 (1972).
[9] G. A. Baker, Jr. and P. Graves-Morris, *Padé Approximants*, 2nd ed. (Cambridge University Press, Cambridge, 1996).
[10] G. A. Baker, Jr., *Essentials of Padé Approximants* (Academic, New York, 1975).
[11] W. H. Press, B. P. Flannery, S. A. Teukolsky, and W. T. Vetterling, *Numerical Recipes* (Cambridge University Press, Cambridge, 1987).
[12] Padé approximant theory appears to be enigmatic see Ref. [9]. There are no known criteria to determine *a priori* if a Padé approximant of a given order will give a successful representation in a given situation.